1 **Catalytic effect of microbially-derived carboxylic acids on the precipitation of**

2 **Mg-calcite and disordered dolomite: Implications for sedimentary dolomite**

3 **formation**

4

5 Deng Liu[1, 2, *], Yangyang Xu[1], Qianqian Yu[3], Na Yu[2], Xuan Qiu[1], Hongmei Wang[1, 2]

6 and Dominic Papineau[1, 4, 5, 6]

7

8 [1]State Key Laboratory of Biogeology and Environmental Geology, China University of

9 Geosciences, Wuhan 430074, China

10 [2]School of Environmental Studies, China University of Geosciences, Wuhan 430074,

11 China

12 [3]School of Earth Sciences, China University of Geosciences, Wuhan 430074, China

13 [4]London Centre for nanotechnology, University College London, 17-19 Gordon

14 Street, London, UK

15 [5]Department of Earth Sciences, University College London, London, UK

16 [6]Center for Planetary Sciences, University College London, London, UK

17

18 Corresponding author:

19 Deng Liu (liud_cug@126.com)

20

23

ABSTRACT

The genesis of dolomite is a contentious issue partly due to the difficulty in its synthesis at ambient temperature. Certain types of microorganisms have been demonstrated to be effective in promoting the precipitation of disordered dolomite, an important precursor of sedimentary ordered dolomite. In contrast to a growing body of research on the catalytic role of microbial exopolymers in the crystallization of disordered dolomite, the role of other microbial exudates (e.g., carboxylic acids) remains unknown. To fill in this knowledge gap, precipitation experiments, mimicking the carbonation process within microbial mats, were conducted in saline solutions containing 0-30 mM succinic acid or citric acid, which are commonly produced by microbes. The starting salinities of experiment solutions were set to 35‰ and 70‰, in order to evaluate the effect of solution salinity on dolomite formation. Our results showed that both succinic acid and citric acid enhanced the incorporation of Mg^{2+} into growing Ca-Mg carbonates. Solution salinity also played a positive role in enhancing Mg signature in Ca-Mg carbonates. Disordered dolomite with 40.92 mol% $MgCO_3$ was detected under the conditions of 30 mM succinic acid and 70‰ salinity, whereas in other reactors with succinic acid, Mg-calcites formed. Citric acid was more effective in loading Mg^{2+} into Ca-Mg carbonates compared with succinic acid, as evidenced by the predominant occurrence of disordered dolomite with $MgCO_3$ content ranging from 40.91 mol% to 46.75 mol% in most conditions tested. The results of this study have implications for the formation mechanism of sedimentary dolomite.

Keywords: dolomite problem; disordered dolomite; carboxylic acid; microbial

46   mediation

47

1. Introduction

49   The mineral dolomite was firstly discovered by Déodat de Dolomieu in 1791 and

50   was later characterized by having a chemical composition of $CaMg(CO_3)_2$ and by

51   consisting of alternating layers of pure Mg and Ca ions separated by layers of CO_3

52   (Gregg et al., 2015). However, it has been recognized that sedimentary dolomite

53   exhibits variations in chemical composition and Ca-Mg order (Land, 1985; Warren,

54   2000). In general, the composition of natural dolomites ranges from $Ca_{1.16}Mg_{0.84}(CO_3)_2$

55   to $Ca_{0.96}Mg_{1.04}(CO_3)_2$ (Warren, 2000). Moreover, dolomite crystals in nature possess

56   partially or fully ordered structure (Goldsmith and Graf, 1958; Land, 1985; Warren,

57   2000; Gregg et al., 2015).

58   Despite the fact that the chemical and textural properties of dolomite have been

59   well studied, the mechanism of its formation remains controversial (Warren, 2000;

60   McKenzie and Vasconcelos, 2009). Such debate, often known as "dolomite problem",

61   was driven by the sharp contrast of the common occurrence of dolomite in pre-

62   Holocene geological records to its paucity in modern sediments and by the difficulty in

63   its synthesis in ambient laboratory settings (Land, 1998; Arvidson and Mackenzie, 1999;

64   Warren, 2000). However, precipitation of dolomite in saturated solution (e.g., modern

65   seawater) is thermodynamically favorable (Given and Wilkinson, 1987). A satisfactory

66   explanation for the scarce occurrence of modern dolomites offered by laboratory

67   experiments further shows that dolomite crystallization is a kinetically-controlled

68   process (Baker and Kastner, 1981; Lippmann, 1982; Shen et al., 2014). Among reported

69   controlling factors, the hydration effect of Mg^{2+} has been recognized as a key kinetic

70   barrier to the incorporation of Mg^{2+} into the lattice of dolomite (Zhang et al., 2012a, b;

71   Shen et al., 2014). Hydrothermal experiments also indicate that the kinetic barrier to

72   dolomite can be overcome at higher temperatures (>100 °C) and disordered dolomite

73   appears as a metastable precursor to dolomite (Malone et al., 1996; Zhang et al., 2010;

74   Rodriguez-Blanco et al., 2015; Kaczmarek and Thornton, 2017). In comparison to

75   dolomite (space group: *R3*), disordered dolomite (whose space group is *R3c*) has near-

76   dolomite stoichiometry (more than 36 mol% and up to ca. 55 mol% $MgCO_3$) but

77   completely disordered Ca-Mg arrangement (Fang and Xu, 2019). On the other hand,

78   disordered dolomite has the same space group as calcite, but its Mg content is higher

79   than that of Mg-calcite (<36 mol% $MgCO_3$) (Fang and Xu, 2019).

80   Although modern dolomite is rarely found in open marine sediments, primary (or

81   very early diagnetic) dolomite precipitates that apparently formed at low temperatures

82   (<60 °C) have been repeatedly observed in highly evaporitic environments (e.g.,

83   Vasconcelos and McKenzie, 1997; Wright, 1999; van Lith et al., 2002, 2003a; Wright

84   and Wacey, 2005; Bontognali et al., 2010, 2012; Deng et al., 2010; Meister et al., 2011;

85   Fang and Xu, 2019; Liu et al., 2019a) and marine cold seeps (e.g., Xu et al., 2010; Lu

86   et al., 2018). These dolomites are normally non-stoichiometric and poorly ordered

87   (Petrash et al., 2017; Fang and Xu, 2019). Laboratory experiments have further shown

88   that the activities of certain types of microorganisms (e.g, sulfate-reducing bacteria,

89   methanogens and halophilic aerobic microbes) are intimately associated with these

4

90   precipitates (Vasconcelos et al., 1995; Warthmann et al., 2000; van Lith et al., 2003b;

91   Roberts et al., 2004; Sánchez-Román et al., 2008, 2009, 2011; Kenward et al., 2009;

92   Xu et al., 2010; Qiu et al., 2017; Liu et al., 2019a). Recently, a growing body of research

93   has revealed the positive role of microbial exopolymers (EPS) in dolomite

94   crystallization (Bontognali et al., 2008, 2014; Krause et al., 2012; Zhang et al., 2015;

95   Liu et al., 2020). Microbial EPS and other biomolecules with high carboxyl-group

96   densities have been demonstrated to effectively diminish the aforementioned hydration

97   effect of Mg^{2+} and thus expedite dolomite precipitation (Kenward et al., 2013; Roberts

98   et al., 2013; Zhang et al., 2015).

99   It is important to note, however, that Gregg et al., (2015) reevaluated the published

100   XRD data of the reportedly microbially-induced dolomites and found that these

101   carbonates actually lack cation ordering. Therefore, disordered dolomite rather than

102   presumably reported dolomite is synthesized by means of microbial mediation (Gregg

103   et al., 2015). Nevertheless, as pointed before, disordered dolomite is considered as the

104   precursor for some ordered dolomites in sedimentary rocks (Warren, 2000; Zhang et al.,

105   2012a, b; Rodriguez-Blanco et al., 2015). In this regards, the contribution of microbes

106   and their organic secretions (e.g., EPS) to the genesis of dolomite in subsurface

107   sediments and sedimentary rocks cannot be ruled out.

108   In addition to the long-chain EPS, microorganisms also secrete copious low-

109   molecular-weight (LMW) organic acids into solution (Sauer et al., 2008). There are

110   several studies that note the positive role of LMW organic acids (e.g., acetate) in the

111   uptake of Mg into growing Mg-calcites (Xu et al., 2010; Zhang et al., 2010). However,

112   it is still unclear whether microbially-derived carboxylic acids can aid in the formation

113   of disordered dolomite. In this study, we examined the synthetic formation of Ca-Mg

114   carbonates using supersaturated solutions containing succinic acid ($C_4H_6O_4$) or citric

115   acid ($C_6H_8O_7$). The reason for these two carboxylic acids tested in this study was that

116   they can be produced by various microorganisms in the tricarboxylic acid cycle (TCA

117   cycle) (Sauer et al., 2008) and thus be virtually found in most aqueous settings,

118   especially within microbial mats where microbial activities are prevalent. Additionally,

119   the effect of salinity on carboxylic acid-mediated precipitation of Ca-Mg carbonates

120   was also evaluated in this study because the salinity in ocean dynamically changed

121   throughout geological history (Knauth, 2005; Hay et al., 2006) and is considered as one

122   of key controls over dolomite crystallization (Folk and Land, 1975). Our results showed

123   that both LMW carboxylic acid and solution salinity could promote the uptake of Mg^{2+}

124   into precipitating Ca-Mg carbonates, thus forming Mg-calcite and even disordered

125   dolomite at 25 °C.

126

127   **2. Materials and methods**

128   **2.1. Synthesis of Ca-Mg carbonates from carboxylic acid-containing solutions and**

129   **chemical analyses**

130   An apparatus using the ammonium carbonate free-drift technique described by

131   Lian et al., (2006) was employed in our experiments. Unlike most conventional

132   methods for synthesizing Ca-Mg carbonates, in which the cations of calcium and

133   magnesium and carbonate anions are mixed instantaneously and simultaneously, the

6

134   minerals in our experiments formed by gradually delivering carbonate into the Ca/Mg

135   solution. The purpose of such operation is mimicking the carbonation process occurring

136   within microbial mats, in which microbial degradation of organic matters (e.g.,

137   proteinaceous substances) could continuously provide NH_4^+ and CO_3^{2-} to benefit the

138   precipitation of Ca-Mg carbonates.

139   Briefly, a number of 100-mL conical glass flasks containing experimental

140   solutions were placed into the upper space of a closed desiccator, along with three

141   underlying beakers each holding 15 g of solid ammonium bicarbonate (NH_4HCO_3). The

142   experimental solutions consisted of 15 mM $CaCl_2$, 90 mM $MgCl_2 \cdot 6H_2O$, different

143   concentrations of succinic or citric acid (0, 5, 10, 20 and 30 mM; Sigma-Aldrich

144   Chemical Company, $\geqslant$ 99.5%) and various amounts of NaCl to obtain starting

145   salinity of 35‰ or 70 ‰. It is relevant to note that the starting Mg/Ca molar ratio is

146   higher than that of modern seawater (6 vs. 5.2), but lies within the range of values

147   measured in present dolomite-forming environments (Table 1 in Deng et al., 2010). The

148   pH of the solutions was adjusted to ~7.50 by addition of 0.5 M NaOH solution. The

149   desiccators were placed in an incubator at 25 °C. Once experiments have been set up,

150   steady-state decomposition of NH_4HCO_3 could provide NH_3 and CO_2 gas, which

151   diffused into the aforementioned solutions and then simultaneously increased solution

152   pH and carbonate alkalinity. As such, growth of Ca-Mg carbonate could occur in the

153   flasks. All experiments were run in duplicates. After two weeks, the precipitates were

154   carefully collected by centrifugation, rinsed three times with doubly distilled water

155   (ddH_2O), and then freeze-dried.

7

156   Solution pH and aqueous Ca^{2+} /Mg^{2+} were measured during carbonation. The pH

157   was determined using a Denver UB-7 pH meter (Denver, USA). The concentrations of

158   Ca^{2+} and Mg^{2+} were analyzed by inductively coupled plasma-optical emission

159   spectrometry (ICP-OES, Thermofisher ICAP6300, USA).

2.2. Preparation of carbonate standards

161   As hydromagnesite [$Mg_5(CO_3)_4(OH)_2 \cdot 4H_2O$] can be easily misidentified as

162   disordered dolomite or dolomite (Zhang et al., 2012a), a hydromagnesite sample,

163   together with inorganic calcite, disordered dolomite and dolomite, was prepared as a

164   standard for inferring the mineralogical composition of our solid products (Liu et al.,

165   2019b). Hydromagnesite was purchased from Xibeili mineral company (Jiangsu, China)

166   (Liu et al., 2019b). The precipitation of calcite was carried out in a glass vessel at 25 °C

167   according to published methodologies (e.g., Butler et al., 2006). Disordered dolomite

168   and dolomite were prepared at 80 °C and 200 °C, respectively, following a reported

169   protocol (Rodriguez-Blanco et al., 2015).

2.3. Mineral analyses

171   Multiple methods were used for mineral analyses. The mineralogical compositions

172   of the precipitates were identified by X-ray diffraction (XRD) and JADE 6 program

173   (MDI, Livermore, USA). Scanning electron microscopy (SEM) and attached energy-

174   dispersive X-ray spectroscopy (EDS) were employed for morphology observations and

175   chemical composition analyses. The crystal structure of precipitates was examined by

176   transmission electron microscopy (TEM) and Raman spectroscopy.

177   Specifically, all XRD analyses were performed using a Scintag X1 X-ray powder

diffractometer (Scintag, Inc., USA) equipped with Cu-Kα radiation at 40 kV and 35

mA. The samples were scanned from 5 to 65° 2θ with a scan rate of 2° 2θ/min. The

$MgCO_3$ contents of Ca-Mg carbonates were calculated from the d-spacing of the (104)

peak by using the calibration curve of Bischoff et al., (1983). The resulting precipitates

were Pt-coated prior to be characterized by a Hitachi SU8010 SEM (Hitachi, Inc.,

Japan). The SEM was operated at an accelerating voltage of 5-15 kV. For the TEM

observations, samples were suspended in ethanol and then pipetted onto 300-mesh

formvar-coated Cu grids. Transmission electron micrographs of the samples were

recorded by a JEOL JEM-2100 LaB6 TEM (JEOL, Japan) with a 200 kV accelerating

voltage. Quantitative EDS and selected area electron diffraction (SAED) were

employed to characterize the individual crystal structure and atomic composition. TEM

images were collected and processed by Gatan DigitalMicrograph software. Raman

spectra were taken by using a RM-1000 laser Raman microscope system (Renishaw,

UK) in the range between 100 and 2000 cm^{-1}. Excitation was with a 20 mW 514.5 nm

Ar^+ laser. The scanning parameter for each spectrum was taken as 10 scans, 10 s per

wavelength on the detector and a 15 μm slit. Spectral peak positions were calibrated

using the 520.5 cm^{-1} line of silicon as a standard.

3. Results

3.1. Changes of aqueous chemistry as a result of carbonation

The NH_4HCO_3 powders were completely decomposed after two weeks. The

reactors with the salinity of 35‰ were selected as representatives to show the time

course changes in aqueous chemistry (Figs. 1 and 2). The pH changes of carboxylic acid-amended systems exhibited a similar trend to those of control reactors (carboxylic acid-free groups): they rapidly increased within the first 10 days and slightly declined afterwards (Figs. 1A and 2A). Similar patterns of calcium removal from solutions were observed in the reactors with or without carboxylic acids (Figs. 1B and 2B), that is, the concentrations of soluble Ca^{2+} ions gradually decrease from ca. 15 mM to near zero by day 14. Unlike Ca^{2+} ions, the changes in concentration of Mg^{2+} were quite different between control and carboxylic acid-amended systems (Figs. 1C and 2C). In general, there was no appreciable Mg^{2+} depletion in control sets. By contrast, the declines in Mg^{2+} ions were observed when carboxylic acids were introduced into the precipitation reactors and these decreases were apparently related to increased dosage of carboxylic acid in solution. Interestingly, citric acid was more effective in removing Mg^{2+} from solutions than succinic acid at the same concentration. Furthermore, in carboxylic acid-amended groups, the concentrations of precipitated Mg (depletion of Mg^{2+}) were linearly correlated with the concentrations of precipitated Ca (Figs. 1D and 2D).

3.2. Characterization of the produced Ca-Mg carbonates

3.2.1. XRD results

During the carbonation process, cloudy solutions were observed within 12 h in the control systems and in 24-48 h in the presence of succinic or citric acids, respectively. Upon crystallization over two weeks, the solid products were collected and then investigated using XRD to probe the effect of LMW carboxylic acids on the crystallization of carbonates. The results showed that the crystals formed in the control

222 systems with salinities of 35‰ and 70 ‰ were exclusively aragonite ($CaCO_3$) (Fig. 3).

223 As expected, the products obtained changed obviously when succinic or citric acid was

224 introduced into the experimental solutions (Figs. 4 and 5). Specifically, the Ca-Mg

225 carbonates of calcite-dolomite series were identified as the major phases, exhibiting the

226 characteristic reflection of a rhombohedral crystal [(hkl) Miller indices: (012), (104),

227 (006), (110), (113), (202), (018), (116), etc.]. In addition to these Ca-Mg carbonates,

228 aragonite and monohydrocalcite ($CaCO_3 \cdot H_2O$) were also produced in some cases.

229 Compared the XRD patterns of Ca-Mg carbonates obtained in each set, shifts in d-

230 spacing could be clearly observed, indicating that different amounts of Mg^{2+} were

231 incorporated into their crystal lattices. To better illustrate the relationship between the

232 concentrations of carboxylic acids and $MgCO_3$ contents in Ca-Mg carbonates, short

233 XRD scans of the (104) reflections for newly formed phases were further obtained (Figs.

234 4 and 5). These XRD profiles revealed that the (104) peak of Ca-Mg carbonate became

235 broader and showed a much higher peak intensity with increasing concentrations of

236 succinic (Figs. 4B and 4D) or citric acid (Figs. 5B and 5D). More interestingly, it also

237 showed that increment in the concentration of these compounds could lead to a

238 progressive decrease in the (104) d-spacing of Ca-Mg carbonate. As clearly shown in

239 Figure 6, the (104) d-spacing (corresponding to mol% $MgCO_3$ in the crystallites) was

240 significantly correlated with the concentration of succinic or citric acid, indicating that

241 these biomolecules are effective in promoting Mg uptake into calcitic structures. It is

242 also interesting to note that the influence of carboxylic acids not only acts in a

243 concentration-dependent fashion, but is also highly dependent on their type. For

244   example, when the solution salinity was 35‰, the carbonates with 8.17, 10.35, 28.91

245   and 33.28 mol% $MgCO_3$ precipitated from solutions with 5, 10, 20 and 30 mM succinic

246   acid, respectively (Bischoff et al., 1983). However, the catalytic effect of citric acid

247   over the same concentration range became more obvious: produced carbonates with an

248   average $MgCO_3$ content of 9.62, 40.92, 42.01 and 44.56 mol%, respectively (Figs. 6B

249   and 6D). Such phenomenon was also found in the experimental systems with the

250   salinity of 70‰. Furthermore, it seems that the elevated salinity of carboxylic acid-

251   bearing solution could also enhance the substitution of Mg for Ca within the resulting

252   carbonate phases, especially those that precipitated from the succinic acid-amended

253   reactors (Fig. 6).

254   According to the terminology proposed by Fang and Xu (2019), the substitution

255   of Mg for Ca sites in calcitic structures can result in four calcite derivatives, including

256   low-Mg calcite (< 4 mol% $MgCO_3$), high-Mg calcite (ranging in content from 4 mol%

257   to 36 mol% $MgCO_3$), disordered dolomite with near-dolomite stoichiometry (more than

258   36 mol% and up to ca. 55 mol% $MgCO_3$) but lacking cation ordering, and dolomite.

259   Employing such criteria, the Ca-Mg carbonates formed in the 5-30 mM succinic acid-

260   amended systems with the salinity of 35‰ had $MgCO_3$ composition ranging from 8.17

261   mol% to 33.28 mol%, corresponding to high-Mg calcite (Fig. 6). Once the salinity of

262   succinic acid-bearing solutions increased up to 70‰, the highest $MgCO_3$ content of Ca-

263   Mg carbonates produced in the solution with 30 mM succinic acid can reach 40.92

264   mol%, close to that of dolomite, while Mg-calcites with $MgCO_3$ content ranging from

265   11.08 mol% to 31.82 mol% precipitated in other systems. As stated before, the $MgCO_3$

266   contents of synthetic Ca-Mg carbonates facilitated by citric acid were significantly

267   higher than those by succinic acid. Ca-Mg carbonates close to dolomite composition

268   (covering the range 40.91-46.75 mol% $MgCO_3$) were produced in the solutions with

269   citric acid over the concentration range of 10-30 mM either at the salinity of 35‰ or at

270   70‰, and Mg-calcites formed when only 5 mM citric acid was used.

271   To exclude the possible misidentification and determine the degree of cation

272   ordering in our organogenic dolomite-like minerals, the XRD reflections of Ca-Mg

273   carbonates induced by 30 mM carboxylic acids, along with inorganically-synthesized

274   disordered dolomite, ordered dolomite, calcite and hydromagnesite, were further shown

275   in Figure 7 for comparison. The XRD pattern and peak position of dolomite-like phases

276   catalyzed by succinic or citric acid were quite similar to those of inorganic disordered

277   dolomite precipitated at 80 °C. In addition, there were no ordering reflections [e.g.,

278   (015), (021), and (101)] in XRD patterns of carboxylic acid-mediated dolomite-like

279   phases. As such, above features indicate that the crystal structure of these dolomite-like

280   materials was highly disordered and thus that they can be identified as disordered

281   dolomite.

282   In summary, these data indicated that (i) both carboxylic acid and salinity had a

283   considerable impact on the Mg^{2+} uptake into calcitic structures, leading to the

284   precipitation of Mg-calcite and even disordered dolomite at ambient temperature; (ii)

285   in comparison to succinic acid, citric acid was more effective in enhancing Mg

286   incorporation into Ca-Mg carbonates.

287   **3.2.2. Micro-Raman analyses**

288   Raman spectra in the range of 130-1200 cm^{-1} were used for interpreting the

289   structural differences among organogenic disordered dolomite, inorganic disordered

290   dolomite and dolomite, and calcite. The spectral bands of rhombohedral crystals in this

291   low-wavenumber region have been widely studied and successful assignments of these

292   vibrations (e.g., Bischoff et al., 1985; Edwards et al., 2005; Perrin et al., 2016).

293   As shown in Figure 8A, similar patterns with four distinct bands were observed in

294   our samples, as consistent with previous studies of carbonate minerals (Bischoff et al.,

295   1985; Perrin et al., 2016). These Raman bands consisted of two lattice modes (i.e., T

296   and L external vibrations) below 350 cm^{-1} that are attributed to motions comprising the

297   complete unit cell (Wehrmeister et al., 2010) and two other internal modes (i.e., v1 and

298   v4), which are due to the symmetric stretching or in-plane bending of the C-O bonds in

299   the carbonate ion (Wehrmeister et al., 2010; Perrin et al., 2016). Specifically for each

300   inorganic standard (Fig. 8A), the peak in the T region was at 155 cm^{-1} for calcite, 173

301   cm^{-1} for disordered dolomite and 175 cm^{-1} for dolomite; the position of the L peak

302   appeared at 281 cm^{-1} for calcite, 297 cm^{-1} for disordered dolomite and 300 cm^{-1} for

303   dolomite; the peak in the v4 region observed for these three phases was at 711, 723 and

304   723 cm^{-1}, respectively; in the v1 cases, the peak position for above standards appeared

305   at 1086, 1095 and 1097 cm^{-1}, respectively. These observations are in good agreement

306   with previous studies (Bischoff et al., 1985; Perrin et al., 2016). In comparison to the

307   standards, the band positions of our carboxylic acid-induced precipitates were much

308   close to that of inorganic disordered dolomite (Fig. 8B), again suggesting that the cation

309   occupancy in the carboxylic acid-catalyzed Ca-Mg carbonate was disordered rather

310 than ordered.

3.2.3. SEM observations

312   The solids produced in our precipitation experiments with 30 mM carboxylic acid

313 at the salinity of 35‰ or 70‰ were selected as representatives for SEM investigation.

314 Mixture-shaped particles with various sizes were obtained under a condition of 30 mM

315 succinic acid and 35‰ salinity (Fig. 9A). These solid phases mainly included elongated

316 rods and spheroidal aggregates (Fig. 9B). The corresponding EDS results (Figs. 9C and

317 9D) revealed that the rod-like microcrystal (particle a in Fig. 9B) contained abundant

318 Ca but negligible Mg, whereas the spheroidal phase (particle b in Fig. 9B) displayed a

319 relatively high Mg/Ca ratio. Combined with XRD data, these two types of solid phases

320 were identified as aragonite and high-Mg calcite. At higher magnification, the

321 submicron-sized spheres were found to be uniformly distributed on the surface of

322 aragonite (Fig. 9E). When the solution salinity was as high as 70‰, more aggregated

323 spheroidal particles were produced in succinic acid-containing solution (Fig. 9F).

324 Detailed observations showed that the spheres had a granular texture itself comprised

325 of many spherical nano-crystals (Fig. 9G). The EDS spectrum (Fig. 9G) showed that

326 these micro-spheroidal neoformations consisted of similar Mg and Ca contents (Kα line

327 area), thus were interpreted as disordered dolomites. SEM images revealed that the

328 solid products in the reactors with 30 mM citric acid were spherulites with averaged

329 size of 2-4 μm (Fig. 10). Based on EDS analyses and XRD results, these spherulites

330 occurring at salinities of 35‰ or 70‰ were identified as disordered dolomites (Fig. 10).

331 Higher magnification images showed that disordered dolomite spherulites were

332   composed of numerous nanoparticles (the inserts in Figs. 10B and 10D), similar to those

333   obtained in succinic acid-bearing systems.

334   **3.2.4. TEM observations**

335   TEM was employed to capture the structure of carbonate minerals occurring in the

336   reactors under a condition of 30 mM carboxylic acid and 35‰ salinity (Figs. 11 and

337   12). The occurrence of rod-like aragonite in succinic acid-containing groups was

338   collectively verified by the results of TEM image, SAED pattern and EDS elemental

339   composition (Figs. 11A-C). In addition to aragonite, high-Mg calcite was also detected

340   (Figs. 11D-G), in good agreement with XRD and SEM results. As shown in Fig. 11D,

341   high-Mg calcite appeared as spheroid-shaped aggregates. High resolution TEM

342   (HRTEM) image further revealed that these nano-sized spheroids were randomly

343   distributed (Fig. 11G).

344   The disordered dolomite crystal obtained from citric acid-containing groups was

345   identified by its morphology and chemical composition from an EDS spectrum (Fig.

346   12A). The disordered dolomite spheroid, when magnified, displayed randomly oriented

347   nano-crystals as shown in Fig. 12B, consistent with the SEM observations (Figs. 10A

348   and 10B). A representative SAED pattern of this sample showed the presence of (104),

349   (110), (113) and (024) reflections but lack of the typical super-lattice reflections [e.g.,

350   (015), (101) and (021)] (the insert in Fig. 12B). Lattice fringe image was further

351   obtained from the edge site of one disordered dolomite particle. It can be found that our

352   synthetic disordered dolomite had a dominant spacing of 0.290 nm, corresponding to

353   the d-spacing of (104) (Fig. 12C).

354

4. Discussion

4.1. The possible role of carboxylic acid in the crystallization of Mg-calcite and disordered dolomite

Many factors control formation of primary Ca-Mg carbonates (e.g., Mg-calcite and disordered dolomite). Once oversaturated condition is achieved, the intrinsic chemical property of Mg^{2+} ion becomes a key factor affecting the growth of Ca-Mg carboantes (Lippman, 1973; de Leeuw and Parker, 2001; Romanek et al., 2009; Shen et al., 2014, 2015). Like Ca^{2+} and other cations, Mg^{2+} ions are strongly hydrated in solution, forming the Mg^{2+}-H_2O complex (i.e., $[Mg(H_2O)_6]^{2+}$) (Lippman, 1973). However, due to the larger hydration enthalpy of Mg^{2+} than that of Ca^{2+} (1926 kJ/mole vs. 1579 kJ/mole) (Lippman, 1973), the occurrence of more stable inner-sphere hydration shell around Mg^{2+} ions not only hinders the adsorption of Mg^{2+} onto crystal surface, but also blocks the subsequent binding of carbonate to surface Mg^{2+} (Shen et al., 2014, 2015). In contrast, it is easier to overcome the hydration barrier surrounding Ca^{2+} ions. Such inhibitory effect of Mg^{2+} hydration on the formation of Ca-Mg carbonates has been demonstrated by several computational studies (e.g., de Leeuw and Parker, 2001; Di Tommaso and de Leeuw, 2010). As such, aragonite (a low-Mg calcium carbonate) rather than Ca-Mg carbonates is the dominant carbonate phase when the Mg/Ca molar ratio of saturated solution exceeds 4.0 (Shen et al., 2014, 2015). Such mechanism helps to explain the paucity of dolomite in marine sediment and the predominant occurrence of aragonite in our control sets.

17

376 A growing body of studies has suggested that microbial EPS could act as natural

377 catalysts to promote the incorporation of Mg^{2+} into growing Ca-Mg carbonates (Zhang

378 et al., 2012a, 2015; Bontognali et al., 2014; Kenward et al., 2013; Liu et al., 2020).

379 Furthermore, carboxyl moieties within EPS matrix were identified as the major

380 functional groups to accelerate Mg^{2+} dehydration (Wang et al., 2009; Roberts et al.,

381 2013; Zhang et al., 2015). Previous studies also proposed that the dehydration reaction

382 induced by carboxyl moieties proceeds possibly via a metal-chelation mechanism

383 (Romanek et al., 2009; Roberts et al., 2013). Specifically, the electronegative carboxyl

384 groups bind to $[Mg(H_2O)_6]^{2+}$ ion pairs and form a $[Mg(H_2O)_5(R\text{-}COO)]^+$ complex,

385 along with the ejection of one water molecule (Roberts et al., 2013). Upon the

386 dewatering, the newly formed Mg-carboxyl complex requires significantly lower

387 energy when binding CO_3^{2-} than $[Mg(H_2O)_6]^{2+}$ (Roberts et al., 2013; Shen et al., 2014).

388 In doing so, it is believed that a thin Ca-Mg carbonate template could form and its

389 growth will take place when a supersaturated condition is maintained (Roberts et al.,

390 2013).

391 Our present study demonstrated that Ca-Mg carbonates occurred in the reactors

392 with succinic acid or citric acid. Given their multicarboxylic status, these two

393 biomolecules may function in the same capacity as EPS through aforementioned model

394 to catalyze the crystallization of Ca-Mg carbonates. This mechanism is likely confirmed

395 by our observation that citric acid displayed more effective in loading Mg^{2+} into

396 growing carbonate, resulting in the formation of disordered dolomite in most conditions

397 tested, because citric acid has higher metal-binding capacity than succinic acid in bulk

398   solutions (binding constants K of citric acid: $K_{Mg}=10^{3.37}$, $K_{Ca}=10^{3.5}$; $K_{succinic\ acid}$:

399    $K_{Mg}=10^{1.2}$, $K_{Ca}=10^{1.2}$) (Cannan and Kibrick, 1938; Wang et al., 2009).

400   In addition to the aforementioned metal-chelation mechanism, the polar behavior

401   of carboxylic acids might also be important for their catalytic role in Ca-Mg carbonate

402   formation. In comparison to water molecules, LMW carboxylic acids typically have a

403   lower dielectric constant (ε). For instance, the ε value of pure succinic acid is 2.4 at

404   20 °C, while water molecular has a value of 80.4 under the same temperature

405   (Kirkwood and Westheimer, 1938). It has been well-known that both water activity and

406   desolvation energy of cations can be reduced by adding a component with a low-

407   dielectric constant (Oomori and Kitano, 1987; Zhang et al., 2012a, b). Furthermore,

408   there have been several studies showing the enhancement of Mg levels in growing Mg-

409   calcite or disordered dolomite by some organic additives that exhibit a low Mg-binding

410   affinity, such as methanol, alcohol, propanol, dioxane, methane, acetate and agar

411   (Oomori and Kitano, 1987; Falini et al., 1996; Xu et al., 2010; Zhang et al., 2010; Zhang

412   et al., 2012a). These organic compounds share the same polar behavior, that is, they all

413   have a low-dielectric constant. As such, it is reasonable to speculate that the effective

414   role of LMW carboxylic acids in the formation of Mg-calcite and disordered dolomite,

415   partly ascribed to their polar behavior, can disturb the association between Mg^{2+} and

416   water dipoles.

417   **4.2. The effect of solution salinity on the formation of Ca-Mg carbonates**

418   In addition to the organic molecules with low-dielectric constant or high Mg^{2+}-

419   binding capacity, there might be some inorganic factors influencing Mg dehydration.

420 Among them, the role of temperature has been long recognized, because the

421 inorganically synthesis of disordered dolomite or dolomite exhibits a positive

422 temperature dependence (e.g., Arvidson and Mackenzie, 1999). Apart from temperature,

423 the importance of solution salinity has been repeatedly underscored by the fact that the

424 formation of Mg calcite and (or) non-stoichiometric dolomite is generally found in

425 hypersaline settings, as stated earlier. One explanation for the positive role of salinity

426 in Ca-Mg carbonate formation is that high salinity itself may directly facilitate the

427 dehydration of Mg^{2+} (Lippman, 1973; Machel and Mountjoy, 1986). Once other cations

428 are dissolved into saturated solution, these cations could also interact with water

429 molecules to form metal-H_2O clusters (e.g., $[Na(H_2O)_n]^+$) (Tsurusawa and Iwata, 1999),

430 possibly disturbing the existing Mg^{2+}-H_2O association. In addition, an indirect effect of

431 salinity has attracted more attention recently. Generally, it is suggested that solution

432 salinity can regulate microbial community composition at first, thus giving rise to the

433 predominance of halophilic microbes, which are thought to be involved in the

434 crystallization of Ca-Mg carbonates, as their cell surface and EPS contain high density

435 of carboxyl groups (Rivadeneyra et al., 2000; Sánchez-Román et al., 2008; Balci and

436 Demirel, 2016; Qiu et al., 2017; Liu et al., 2019a).

437 Our present results showed that solution salinity had a considerable influence on

438 the formation of Ca-Mg carbonates in the abiotic reactors, perhaps supporting its direct

439 impact on the disturbance of Mg^{2+}-H_2O association. However, further computational

440 studies are warranted to completely verify such hypothesis.

441 **4.3. Geological implications**

442   Our results revealed that microbially-derived carboxylic acids were effective in

443   diminishing the hydration effect of Mg^{2+} and thus promoting the incorporation of Mg^{2+}

444   into growing Ca-Mg carbonates. Carboxylic acids are ubiquitous and important

445   components of the aquatic systems, which have been detected in some seawaters and

446   marine porewaters at concentrations of up to ~ 3 mM (Albert and Martens, 1997).

447   Within microbial mats of evaporated saline deposits (e.g., coastal lagoons, brackish and

448   saline lakes), the concentration of carboxylic acids should be higher, because

449   microorganisms usually produce carboxyl-rich compounds to maintain their metabolic

450   functions in the presence of high concentration of salts (Fukuchi et al., 2003; DasSarma,

451   2006). Even if the concentration of LMW carboxylic acids in microbial mats are not as

452   high as the ones we tested herein, these compounds, together with other microbial

453   exudates (e.g., EPS), might play an important role in the formation of disordered

454   dolomite. Once disordered dolomite has formed, it undergoes an "ageing" process upon

455   burial and converts to well-crystallized ordered dolomite, as documented in previous

456   work (Malone et al., 1996; Warren, 2000; Bontognali et al., 2014; Rodriguez-Blanco et

457   al., 2015). As such, a two-stage model, which begins with the precipitation of

458   disordered dolomite via microbial exudates (EPS and LMW carboxylic acids) followed

459   by subsequent diagenetic transformation of disordered dolomite to ordered dolomite,

460   provides one possible interpretation on the occurrence of dolomite in modern

461   hypersaline environments. Indeed, a field investigation conducted by Bontognali et al.

462   (2010) showed that authigenic dolomites in the sabkha of Abu Dhabi exclusively

463   occurred within the buried microbial mats, in which the concentration of microbial

464   exudates was apparently higher than that in non-mat sediments. Such model might also

465   explain dolomite formation in the ancient sea. It has been postulated that the ocean

466   salinity in the Precambrian, the "age of microorganisms", was in the range of 40-70‰,

467   significantly higher than that of modern ocean (~29‰) (Knauth, 2005). The high

468   salinity is able to not only initiate the dehydration of $Mg-H_2O$ complexes both directly

469   and indirectly, but also decrease oxygen solubility in seawater (Knauth, 2005) that

470   benefits the preservation of microbial exudates and dolomite precipitation.

471

472 **5. Conclusion**

473   We demonstrated that the incorporation of Mg^{2+} into growing Ca-Mg carbonates

474   in saline solutions could be enhanced by succinic and citric acid and the incorporation

475   amounts of Mg^{2+} was correlated with the concentration of carboxylic acids and solution

476   salinity. Disordered dolomites were observed when both 30 mM succinic acid and

477   salinity level of 70‰ were used, in most systems with citric acid as confirmed by XRD

478   patterns, Raman spectra and TEM-SAED. Considering the wide distribution of

479   carboxylic acids and other microbial exudates (e.g., EPS) in natural environments and

480   high salinity in evaporitic conditions, the microbial exudate-mediated dolomite

481   formation offers one overlooked possibility for the occurrence of dolomite in Holocene

482   sediments and sedimentary rocks.

483

492

References

494 Albert, D.B., Martens, C.S., 1997. Determination of low-molecular-weight organic acid

495   concentrations in seawater and pore-water samples via HPLC. Mar. Chem.

496   56(1-2), 27-37.

497 Arvidson, R.S., Mackenzie, F.T., 1999. The dolomite problem: control of precipitation

498   kinetics by temperature and saturation state. Am. J. Sci. 299(4), 257-288.

499 Baker, P.A., Kastner, M., 1981. Constraints on the formation of sedimentary dolomite.

500   Science, 213(4504), 214-216.

501 Balci, N., Demirel, C., 2016. Formation of carbonate nanoglobules by a mixed natural

502   culture under hypersaline conditions. Minerals 6(4), 122.

503 Bischoff, W.D., Bishop, F.C., Mackenzie, F.T., 1983. Biogenically produced magnesian

504   calcite: inhomogeneities in chemical and physical properties; comparison with

505   synthetic phases. Am. Mineral. 68(11-12), 1183-1188.

506 Bischoff, W.D., Sharma, S.K., MacKenzie, F.T., 1985. Carbonate ion disorder in

507   synthetic and biogenic magnesian calcites: a Raman spectral study. Am. Mineral.

70(5-6), 581-589.

Bontognali, T.R.R., Vasconcelos, C., Warthmann, R.J., Dupraz, C., Bernasconi, S.M., McKenzie, J.A., 2008. Microbes produce nanobacteria-like structures, avoiding cell entombment. Geology 36(8), 663-666.

Bontognali, T.R.R., Vasconcelos, C., Warthmann, R.J., Bernasconi, S.M., Dupraz, C., Stohmenger, C.J., McKenzie, J.A., 2010. Dolomite formation within microbial mats in the coastal sabkha of Abu Dhabi (United Arab Emirates). Sedimentology 57(3), 824-844.

Bontognali, T.R., Vasconcelos, C., Warthmann, R.J., Lundberg, R., McKenzie, J.A., 2012. Dolomite-mediating bacterium isolated from the sabkha of Abu Dhabi (UAE). Terra Nova 24(3), 248-254.

Bontognali, T.R., McKenzie, J.A., Warthmann, R.J., Vasconcelos, C., 2014. Microbially influenced formation of Mg-calcite and Ca-dolomite in the presence of exopolymeric substances produced by sulphate-reducing bacteria. Terra Nova 26(1), 72-77.

Butler, M.F., Glaser, N., Weaver, A.C., Kirkland, M., Heppenstall-Butler, M., 2006. Calcium carbonate crystallization in the presence of biopolymers. Cryst. Growth Des. 6(3), 781-794.

Cannan, R.K., Kibrick, A., 1938. Complex formation between carboxylic acids and divalent metal cations. J. Am. Chem. Soc. 60(10), 2314-2320.

DasSarma, S., 2006. Extreme halophiles are models for astrobiology. Microbe 1(3), 120.

de Leeuw, N.H., Parker, S.C., 2001. Surface-water interactions in the dolomite problem.

530   Phys. Chem. Chem. Phys. 3(15), 3217-3221.

531   Deng, S., Dong, H., Lv, G., Jiang, H., Yu, B., Bishop, M.E., 2010. Microbial dolomite

532   precipitation using sulfate reducing and halophilic bacteria: Results from

533   Qinghai Lake, Tibetan Plateau, NW China. Chem. Geol. 278(3), 151-159.

534   Di Tommaso, D., de Leeuw, N.H., 2010. Structure and dynamics of the hydrated

535   magnesium ion and of the solvated magnesium carbonates: insights from first

536   principles simulations. Phys. Chem. Chem. Phys. 12(4), 894-901.

537   Edwards, H.G., Villar, S.E.J., Jehlicka, J., Munshi, T., 2005. FT-Raman spectroscopic

538   study of calcium-rich and magnesium-rich carbonate minerals. Spectrochim.

539   Acta A 61(10), 2273-2280.

540   Falini, G., Gazzano, M., Ripamonti, A., (1996) Magnesium calcite crystallization from

541   water-alcohol mixtures. Chem. Commun. 9, 1037-1038.

542   Fang, Y., Xu, H., (2019) A new approach to quantify the ordering state of protodolomite

543   using XRD, TEM, and Z-contrast imaging. J. Sediment. Res. 89, 537-551.

544   Folk, R.L., Land, L.S., (1975) Mg/Ca ratio and salinity: two controls over

545   crystallization of dolomite. AAPG Bull. 59(1), 60-68.

546   Fukuchi, S., Yoshimune, K., Wakayama, M., Moriguchi, M., Nishikawa, K., 2003.

547   Unique amino acid composition of proteins in halophilic bacteria. J. Mol. Biol.

548   327(2), 347-357.

549   Given, R.K., Wilkinson, B.H, 1987. Dolomite abundance and stratigraphic age:

550   constraints on rates and mechanisms of Phanerozoic dolostone formation:

551   Perspectives. J. Sediment. Petrol. 57(6), 1068-1078.

Goldsmith, J.R., Graf, D.L., 1958. Structural and compositional variations in some natural dolomites. J. Geol. 66(6), 678-693.

Gregg, J.M., Bish, D.L., Kaczmarek, S.E., Machel, H.G., 2015. Mineralogy, nucleation and growth of dolomite in the laboratory and sedimentary environment: a review. Sedimentology 62(6), 1749-1769.

Hay, W.W., Migdisov, A., Balukhovsky, A.N., Wold, C.N., Flögel, S., Söding, E., 2006. Evaporites and the salinity of the ocean during the Phanerozoic: Implications for climate, ocean circulation and life. Palaeogeogr. Palaeochimatol. Palaeoecol. 240(1), 3-46.

Kenward, P., Goldstein, R., Gonzalez, L., Roberts, J., 2009. Precipitation of low-temperature dolomite from an anaerobic microbial consortium: the role of methanogenic Archaea. Geobiology 7(5), 556-565.

Kenward, P.A., Fowle, D.A., Goldstein, R.H., Ueshima, M., González, L.A., Roberts, J.A., 2013. Ordered low-temperature dolomite mediated by carboxyl-group density of microbial cell walls. AAPG Bull. 97(11), 2113-2125.

Kirkwood, J., Westheimer, F., 1938. The electrostatic influence of substituents on the dissociation constants of organic acids. I. J. Chem. Phys. 6(9), 506-512.

Knauth, L.P., 2005. Temperature and salinity history of the Precambrian ocean: implications for the course of microbial evolution. Palaeogeogr. Palaeochimatol. Palaeoecol. 219(1), 53-69.

Krause, S., Liebetrau, V., Gorb, S., Sánchez-Román, M., McKenzie, J.A., Treude, T., 2012. Microbial nucleation of Mg-rich dolomite in exopolymeric substances

under anoxic modern seawater salinity: new insight into an old enigma. Geology 40(7), 587-590.

Land, L.S., 1985. The origin of massive dolomite. J. Geol. Educ. 33(2), 112-125.

Land, L.S., 1998. Failure to precipitate dolomite at 25 °C from dilute solution despite 1000-fold oversaturation after 32 years. Aquat. Geochem. 4(3), 361-368.

Lian, B., Hu, Q., Chen, J., Ji, J., Teng, H.H., 2006. Carbonate biomineralization induced by soil bacterium Bacillus megaterium. Geochim. Cosmochim. Acta 70(22), 5522-5535.

Lippmann, F., 1973. Crystal chemistry of sedimentary carbonate minerals, Sedimentary Carbonate Minerals. Springer, pp. 5-96.

Lippman, F., 1982. Stable and metastable solubility diagrams for the system $CaCO_3$-$MgCO_3$-H_2O at ordinary temperatures. Bull. Mineral. 105, 273-279.

Liu, D., Xu, Y., Papineau, D., Yu, D., Fan, Q., Qiu, X., Wang, H., 2019a. Experimental evidence for abiotic formation of low-temperature proto-dolomite facilitated by clay minerals. Geochim. Cosmochim. Acta 247, 83-95.

Liu, D., Yu, N., Papineau, D., Fan, Q., Wang, H., Qiu , X., She, Z., Luo, G., 2019b. The catalytic role of planktomic aerobic heterotrophic bacteria in protodolomite formation: Results from Lake Jibuhulangtu Nuur, Inner Mongolia, China. Geochim. Cosmochim. Acta 263, 31-49.

Liu, D., Fan, Q., Papineau, D., Yu, N., Chu, Y., Wang, H., Qiu, X., Wang, X., 2020. Precipitation of protodolomite facilitated by sulfate-reducing bacteria: The role of capsule extracellular polymeric substances. Chem. Geol. 533, 119415.

596   Lu, Y., Sun, X., Xu, H., Konishi, H., Lin, Z., Xu, L., Chen, T., Hao, X., Lu, H.,

597   Peckmann, J., 2018. Formation of dolomite catalyzed by sulfate-driven anerobic

598   oxidation of methane: Mineralogical and geochemical evidence from the

599   northern South China Sea. Am. Mineral. 103, 720-734.

600   Machel, H.G., Mountjoy, E.W., 1986. Chemistry and environments of dolomitization-

601   a reappraisal. Earth Sci. Rev. 23(3), 175-222.

602   Malone, M.J., Baker P.A., Burns S.J., 1996. Recrystallization of dolomite: An

603   experimental study from. Geochim. Cosmochim. Acta 60(12), 2189-2207.

604   McKenzie, J.A., Vasconcelos, C., 2009. Dolomite Mountains and the origin of the

605   dolomite rock of which they mainly consist: historical developments and new

606   perspectives. Sedimentology 56(1), 205-219.

607   Meister, P., Reyes, C., Beaumont, W., Rincon, M., Collins, L., Berelson, W., Stott, L.,

608   Corserrri, F., Nealson, K.H., 2011. Calcium and magnesium-limited dolomite

609   precipitation at Deep Springs Lake, California. Sedimentology 58(7),   1810-

610   1830.

611   Oomori, T., Kitano, Y., 1987. Synthesis of protodolomite from sea water containing

612   dioxane. Geochem. J. 21(2), 59-65.

613   Perrin, J., Vielzeuf, D., Laporte, D., Ricolleau, A., Rossman, G.R., Floquet, N., 2016.

614   Raman characterization of synthetic magnesian calcites. Am. Mineral. 101(11),

615   2525-2538.

616   Petrash, D.A., Bialik, O.M., Bontognali, T.R.R., Vasconcelos, C., Roberts, J.A.,

617   McKenzie, J.A., Konhauser, K.O., 2017. Microbially catalyzed dolomite

618   formation: From near-surface to burial. Earth-Sci. Rev. 171, 558-582.

619 Qiu, X., Wang, H., Yao, Y., Duan, Y., 2017. High salinity facilitates dolomite

620   precipitation mediated by Haloferax volcanii DS52. Earth Planet. Sci. Lett. 472,

621   197-205.

622 Rivadeneyra, M.A.A., Delgado, G., Soriano, M., Ramos-Cormenzana, A., Delgado, R.,

623   2000. Precipitation of carbonates by Nesterenkonia halobia in liquid media.

624   Chemosphere 41(4), 617-624.

625 Roberts, J.A., Bennett, P.C., González, L.A., Macpherson, G., Milliken, K.L., 2004.

626   Microbial precipitation of dolomite in methanogenic groundwater. Geology,

627   32(4), 277-280.

628 Roberts, J.A., Kenward, P.A., Fowle, D.A., Goldstein, R.H., González, L.A., Moore,

629   D.S., 2013. Surface chemistry allows for abiotic precipitation of dolomite at low

630   temperature. Proc. Natl. Acad. Sci. 110(36), 14540-14545.

631 Rodriguez-Blanco, J.D., Shaw, S., Benning, L.G., 2015. A route for the direct

632   crystallization of dolomite. Am. Mineral. 100(5-6), 1172-1181.

633 Romanek, C.S., Jiménez-López, C., Navarro, A.R., Sánchez-Román, M., Sahai, N.

634   Coleman, M., 2009. Inorganic synthesis of Fe-Ca-Mg carbonates at low

635   temperature. Geochim. Cosmochim. Acta 73(18), 5361-5376.

636 Sánchez-Román, M., Vasconcelos, C., Schmid, T., Dittrich, M., McKenzie, J.A., Zenobi,

637   R., Rivadeneyra, M.A., 2008. Aerobic microbial dolomite at the nanometer

638   scale: Implications for the geologic record. Geology 36(11), 879-882.

639 Sánchez-Román, M., McKenzie, J.A., Wagener, A.D.L.R., Rivadeneyra, M.A.,

640   Vasconcelos, C., 2009. Presence of sulfate does not inhibit low-temperature

641   dolomite precipitation. Earth Planet. Sci. Lett. 285(1), 131-139.

642 Sánchez-Román, M., McKenzie, J.A., de Luca Rebello Wagener, A., Romanek, C.S.,

643   Sánchez-Navas, A., Vasconcelos, C., 2011. Experimentally determined

644   biomediated Sr partition coefficient for dolomite: Significance and implication

645   for natural dolomite. Geochim. Cosmochim. Acta 75(3), 887-904.

646 Sauer, M., Porro, D., Mattanovich, D., Branduardi, P., 2008. Microbial production of

647   organic acids: expanding the markets. Trends Biotechnol. 26(2), 100-108.

648 Shen, Z., Liu, Y., Brown, P.E., Szlufarska, I., Xu, H., 2014. Modeling the effect of

649   dissolved hydrogen sulfide on Mg^{2+}-water complex on dolomite {104} surfaces.

650   J. Phys. Chem. C 118, 15716-15722.

651 Shen, Z., Brown, P.E., Szlufarska, I., Xu, H., 2015. Investigation of the role of

652   polysaccharide in the dolomite growth at low temperature by using atomistic

653   simulations. Langmuir 31(38), 10435-10442.

654 Tsurusawa, T., Iwata, S., 1999. Theoretical studies of strucrues and ioniization threshold

655   energies of water cluster complexes with a group 1 metal, $M(H_2O)_n$ (M=Li and

656   Na). J. Phys. Chem. A 103, 6134-6141.

657 van Lith, Y., Vasconcelos, C., Warthmann, R., Martins, J., McKenzie, J., 2002. Bacterial

658   sulfate reduction and salinity: two controls on dolomite precipitation in Lagoa

659   Vermelha and Brejo do Espinho (Brazil). Hydrobiologia 485(1), 35-49.

660 van Lith, Y., Warthmann, R., Vasconcelos, C., McKenzie, J.A., 2003a. Microbial

661   fossilization in carbonate sediments: a result of the bacterial surface

662   involvement in dolomite precipitation. Sedimentology 50(2), 237-245.

663   van Lith, Y., Warthmann, R., Vasconcelos, C., Mckenzie, J.A., 2003b. Sulphate-

664   reducing bacteria induce low-temperature Ca-dolomite and high Mg-calcite

665   formation. Geobiology 1(1), 71-79.

666   Vasconcelos, C., McKenzie, J.A., Bernasconi, S., Grujic, D., Tiens, A.J., 1995.

667   Microbial mediation as a possible mechanism for natural dolomite formation at

668   low temperatures. Nature 377(6546), 220-222.

669   Vasconcelos, C., McKenzie, J.A., 1997. Microbial mediation of modern dolomite

670   precipitation and diagenesis under anoxic conditions (Lagoa Vermelha, Rio de

671   Janeiro, Brazil). J. Sediment. Res. 67(3), 378-390.

672   Wang, D., Wallace, A.F., De Yoreo, J.J., Dove, P.M., 2009. Carboxylated molecules

673   regulate magnesium content of amorphous calcium carbonates during

674   calcification. Proc. Natl. Acad. Sci. 106(51), 21511-21516.

675   Warren, J., 2000. Dolomite: occurrence, evolution and economically important

676   associations. Earth-Sci. Rev. 52(1), 1-81.

677   Warthmann, R., Van Lith, Y., Vasconcelos, C., McKenzie, J.A., Karpoff, A.M., 2000.

678   Bacterially induced dolomite precipitation in anoxic culture experiments.

679   Geology 28(12), 1091-1094.

680   Wehrmeister, U., Soldati, A., Jacob, D., Häger, T., Hofmeister, W., 2010. Raman

681   spectroscopy of synthetic, geological and biological vaterite: a Raman

682   spectroscopic study. J. Raman Spectrosc. 41(2), 193-201.

683   Wright, D.T., 1999. The role of sulphate-reducing bacteria and cyanobacteria in

684   dolomite formation in distal ephemeral lakes of the Coorong region, South

685   Australia. Sediment. Geol. 126(1), 147-157.

686   Wright, D.T., Wacey, D., 2005. Precipitation of dolomite using sulphate-reducing

687   bacteria from the Coorong Region, South Australia: significance and

688   implications. Sedimentology 52(5), 987-1008.

689   Xu, H., 2010. Synergistic roles of microorganisms in mineral precipitates associated

690   with deep sea methane seeps. In Barton, L.L., Mandl, M., Loy, A., Eds.,

691   Geomicrobiology: Molecular and Environmental Perspective, 325-346.

692   Springer, Berlin.

693   Zhang, F., Xu, H., Konishi, H., Roden, E.E., 2010. A relationship between d_{104} value

694   and composition in the calcite-disordered dolomite solid-solution series. Am.

695   Mineral. 95, 1650-1656.

696   Zhang, F., Xu, H., Konishi, H., Shelobolina, E.S., Roden, E., 2012a. Polysaccharide-

697   catalyzed nucleation and growth of disordered dolomite: A potential precursor

698   of sedimentary dolomite. Am. Mineral. 97(4), 556-567.

699   Zhang, F., Xu, H., Konishi, H., Kemp, J.M., Roden, E.E., Shen, Z., 2012b. Dissolved

700   sulfide-catalyzed precipitation of disordered dolomite: Implications for the

701   formtion mechanism of sedimentary dolomite. Geochim. Cosmochim. Acta

702   97, 148-165.

703   Zhang, F., Xu, H., Shelobolina, E.S., Konishi, H., Converse, B., Shen, Z., Roden, E.E.,

704   2015. The catalytic effect of bound extracellular polymeric substances excreted

705   by anaerobic microorganisms on Ca-Mg carbonate precipitation: Implications

706 for the "dolomite problem". Am. Mineral. 100(2-3), 483-494.

707

Figure caption:

Figure 1. Aqueous chemistry data with time in the experiments with 30 mM succinic acid (SA) at the salinity of 35‰: (A) pH; (B) soluble Ca; (C) soluble Mg; (D) precipitated Ca vs. precipitated Mg.

Figure 2. Aqueous chemistry data with time in the experiments with 30 mM citric acid (CA) at the salinity of 35‰: (A) pH; (B) soluble Ca; (C) soluble Mg; (D) precipitated Ca vs. precipitated Mg.

Figure 3. XRD patterns of solid products in the control systems at the salinities of 35‰ and 70‰.

Figure 4. XRD patterns of minerals obtained from the reactors with 5-30 mM succinic acid: (A) results for the sets at 35‰ salinity and (B) enlarged and smoothed patterns for the (104) reflection; (C) results for the sets at 70‰ salinity and (D) enlarged and smoothed patterns for the (104) reflection (A, aragonite; M, monohydrocalcite).

Figure 5. XRD patterns of minerals grown in the presence of different concentrations of citric acid: (A) results for the sets at 35‰ salinity and (B) enlarged and smoothed patterns for the (104) reflection; (C) results for the sets at 70‰ salinity and (D) enlarged and smoothed patterns for the (104) reflection (A, aragonite; M, monohydrocalcite).

Figure 6. Plots showing the relationships of carboxylic acid concentration with the (104) d-spacing of Ca-Mg carbonate and with the Mg content in Ca-Mg carbonate: (A-B) succinic acid sets; (C-D) citric acid sets.

Figure 7. (A) Comparison of the XRD patterns from organogenic disordered dolomites, inorganically-synthesized disordered and ordered dolomite, calcite and hydromagnesite (SA, succinic acid; CA, citric acid).

Figure 8. (A) Raman spectra of organogenic disordered dolomites and inorganic carbonate standards: a-c, disordered dolomites synthesized with aid of 30 mM succinic acid (35‰ salinity), 30 mM citric acid and salinity of 35‰, and 30 mM citric acid and salinity of 70‰, respectively; d, inorganic disordered dolomite; e, calcite; f, ordered dolomite. (B) Comparison of the Raman bands from organogenic disordered dolomites and inorganic carbonate standards.

Figure 9. SEM images and SEM-EDS composition show the solid products in the systems with 30 mM succinic acid: (A-E) under the salinity level of 35‰; (F-G) with salinity of 70‰. The Pt peak in the EDS spectra came from sampling coating.

Figure 10. SEM images and SEM-EDS composition show the solid products in the solutions with 30 mM citric acid and salinities of 35‰ (A-B) or 70‰ (C-D).

Figure 11. TEM micrographs, EDS composition and SAED pattern for minerals obtained from the system amended with 30 mM succinic acid: (A-C) aragonite; (D-G) Mg-calcite.

Figure 12. TEM micrographs, EDS composition and SAED pattern for minerals obtained from the system amended with 30 mM citric acid: (A) aggregates of disordered dolomite spheroid; (B) disordered dolomite spheroid consisting of many nanocrystallites; (C) a high-resolution image of disordered dolomite displaying a 0.290 nm lattice fringe, corresponding to d-sapcing of (104). The Cu signal in EDS spectrum is attributed to the copper mesh for TEM.
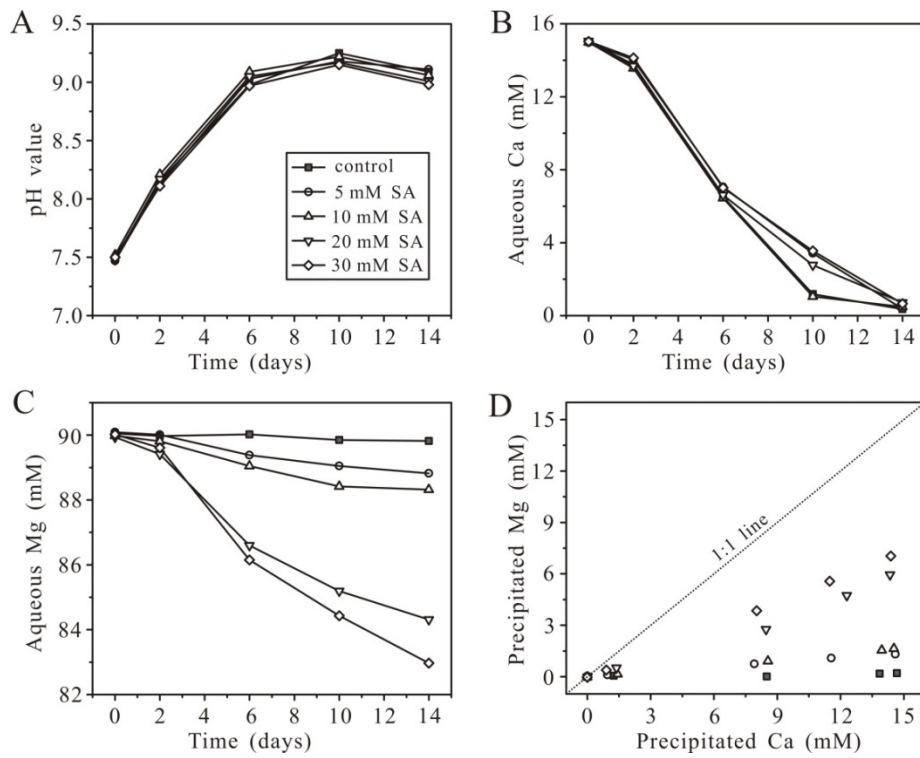
Figure 1
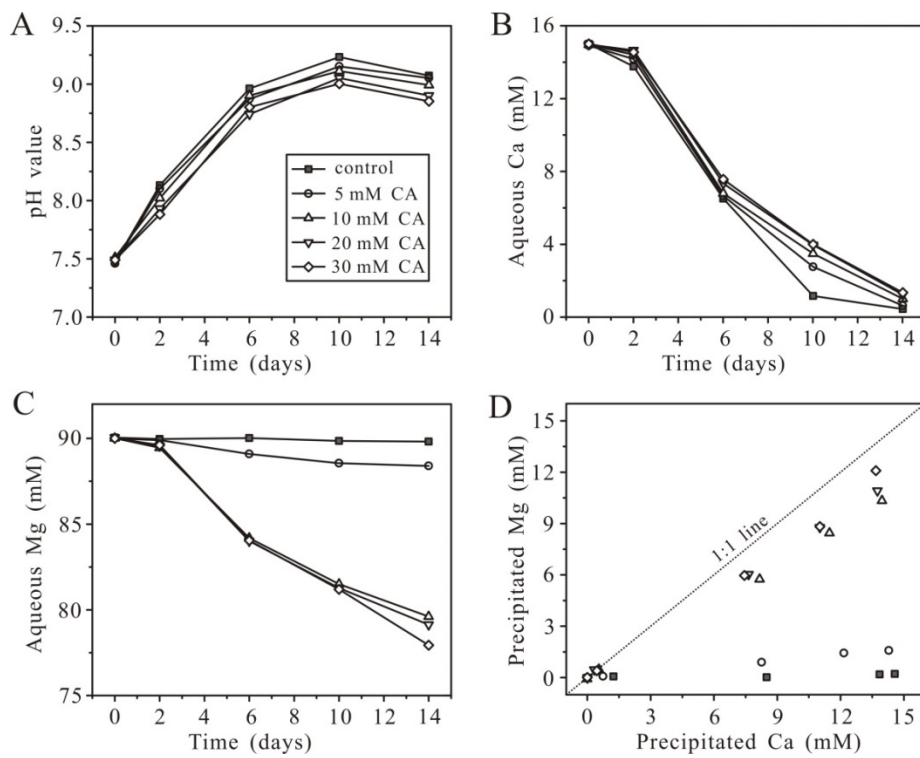
Figure 2
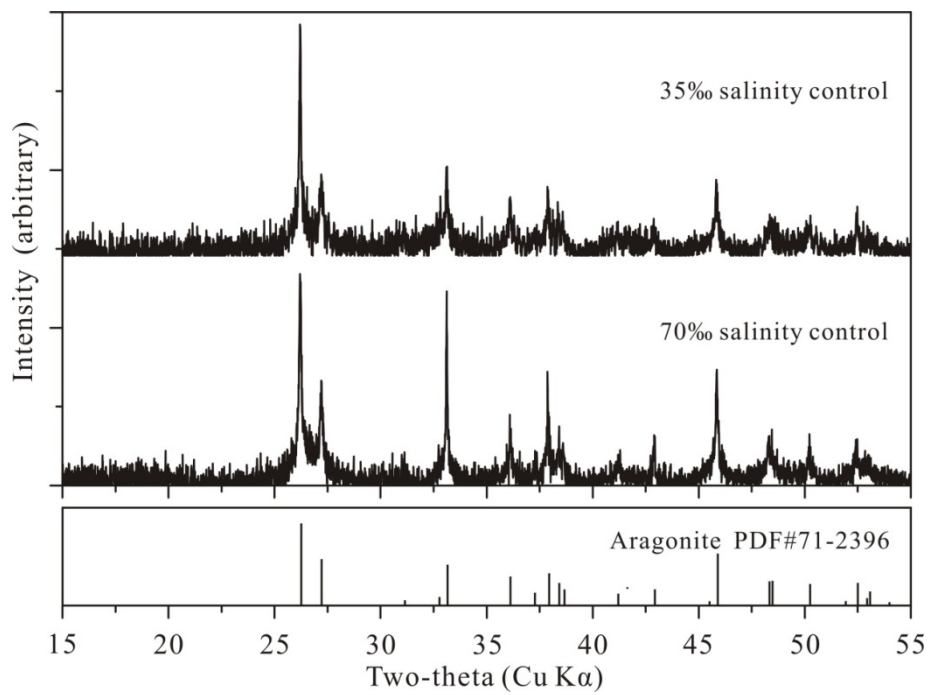
Figure 3
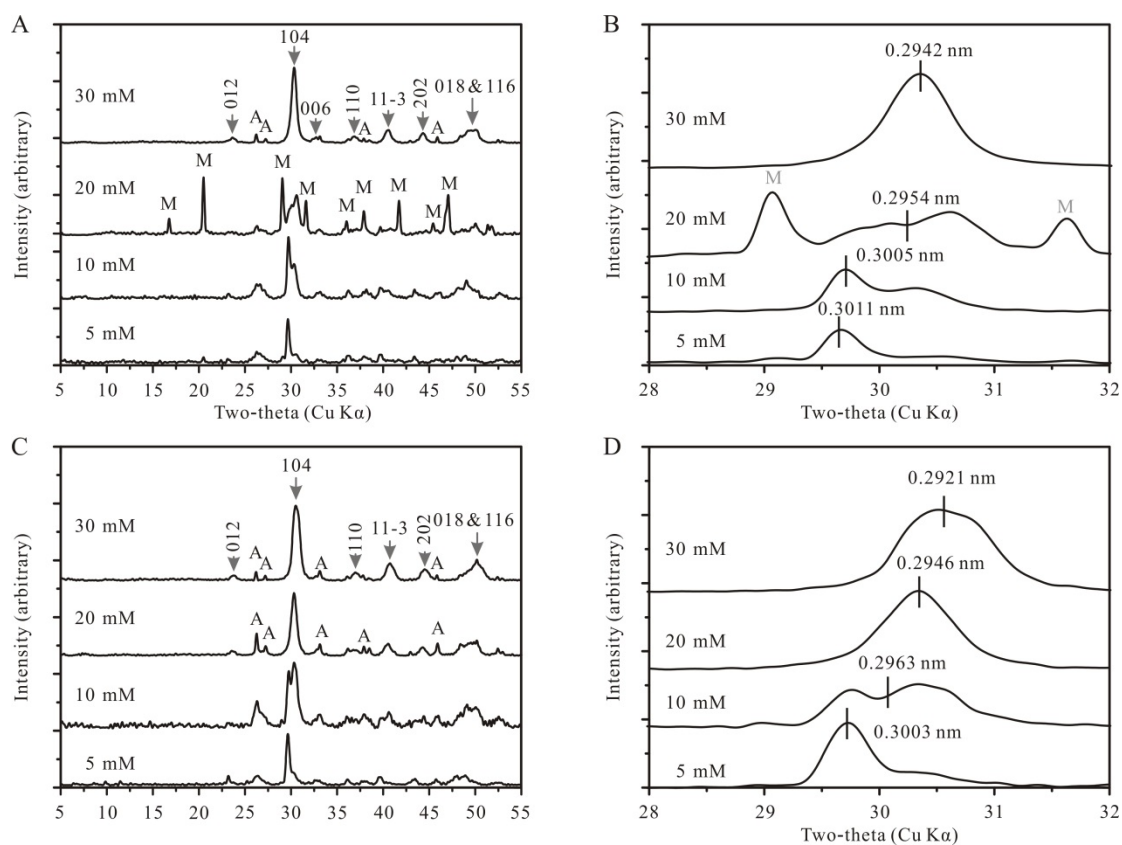
Figure 4
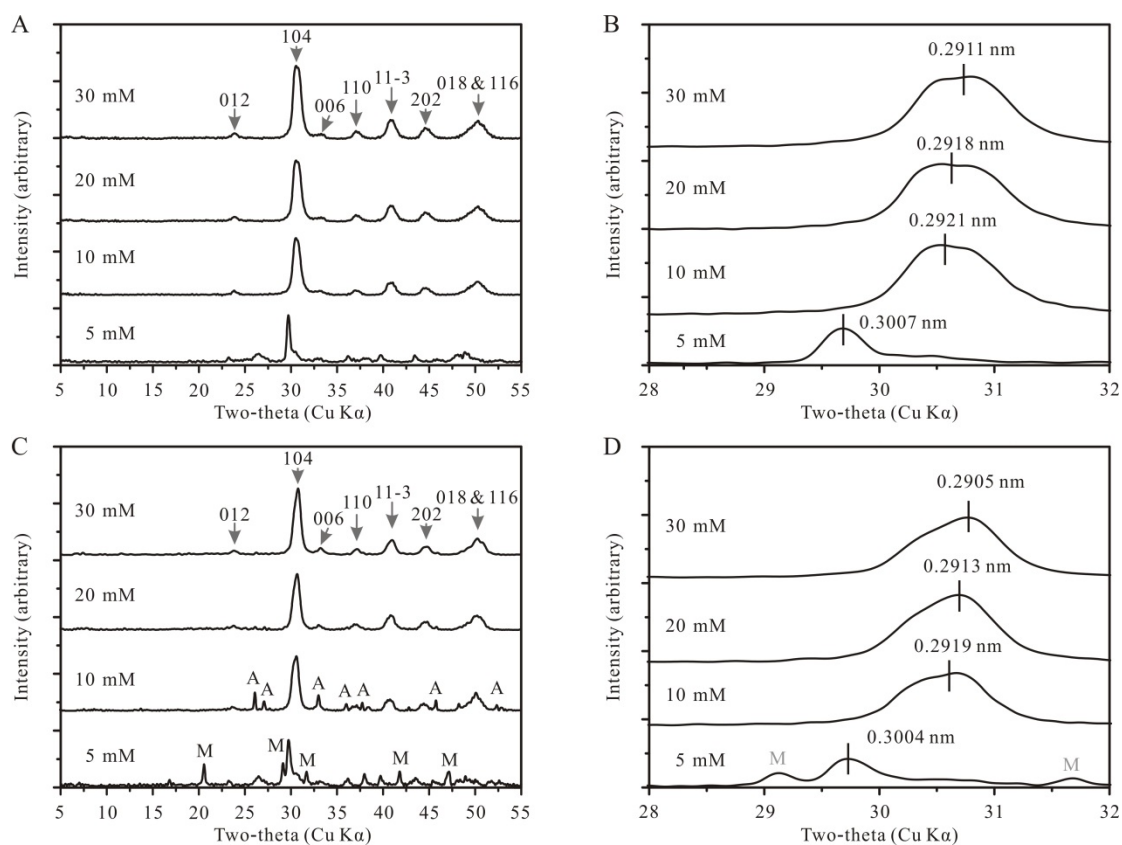
Figure 5
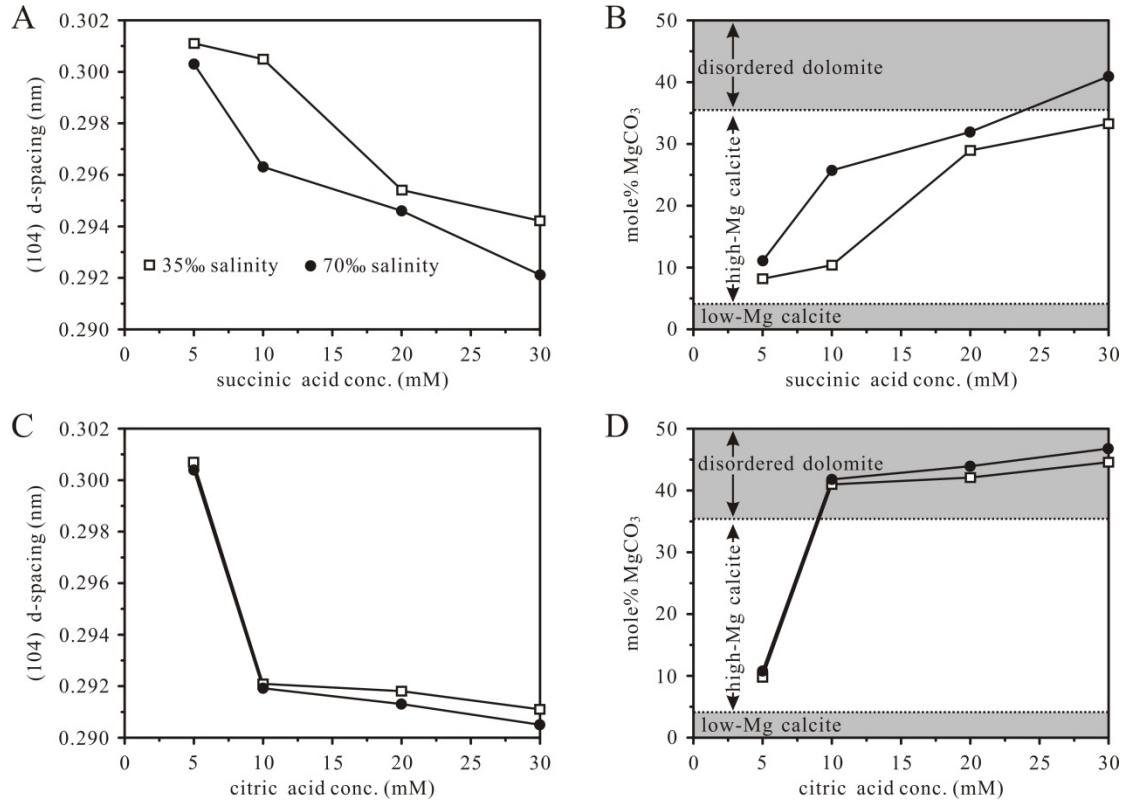
Figure 6
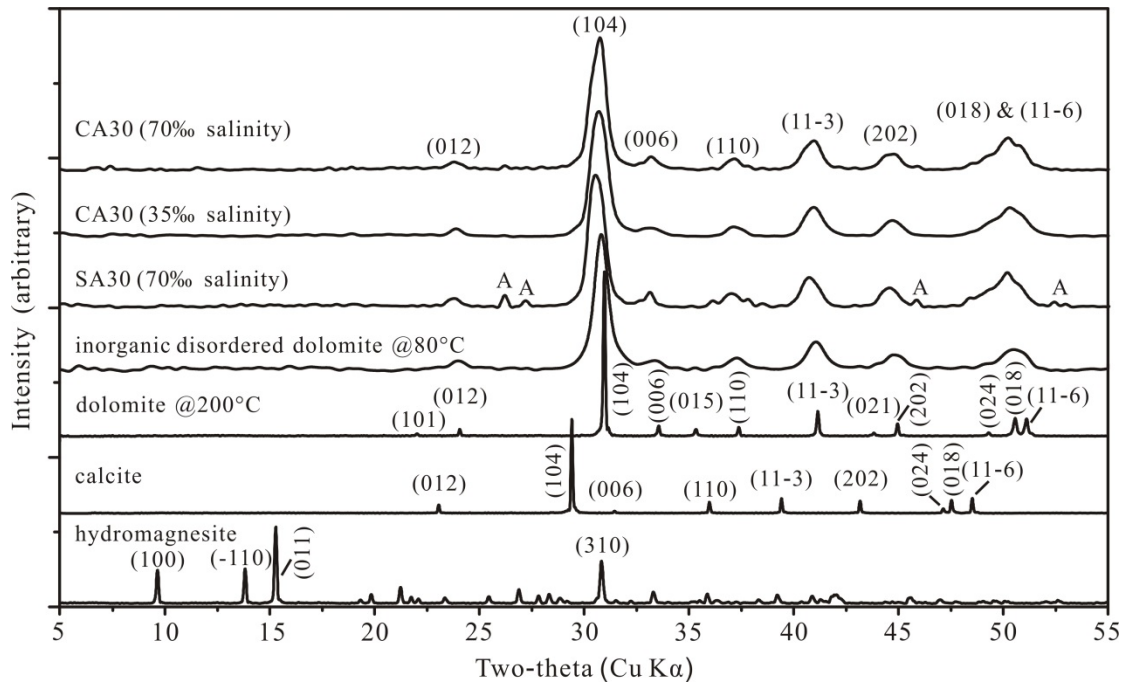
Figure 7
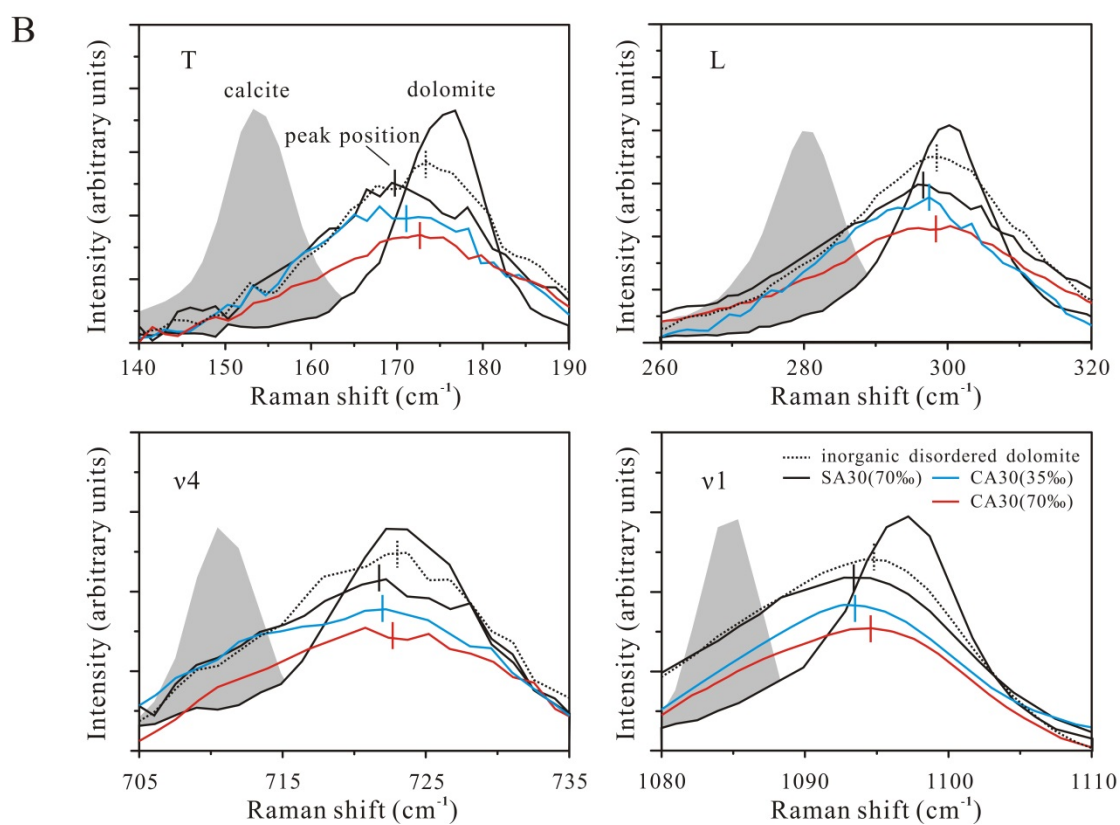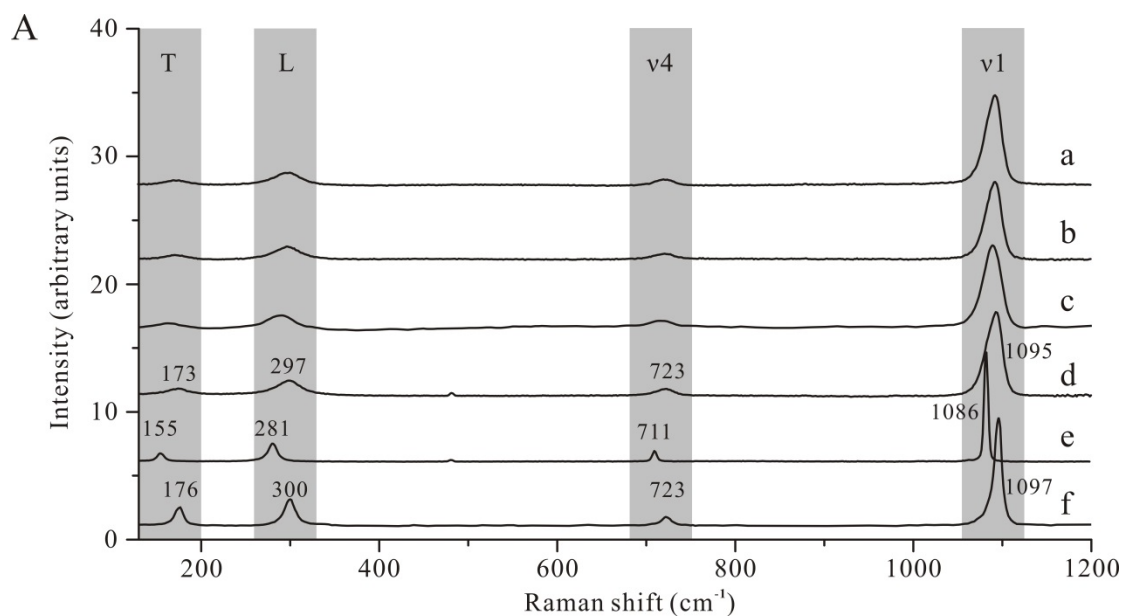
Figure 8
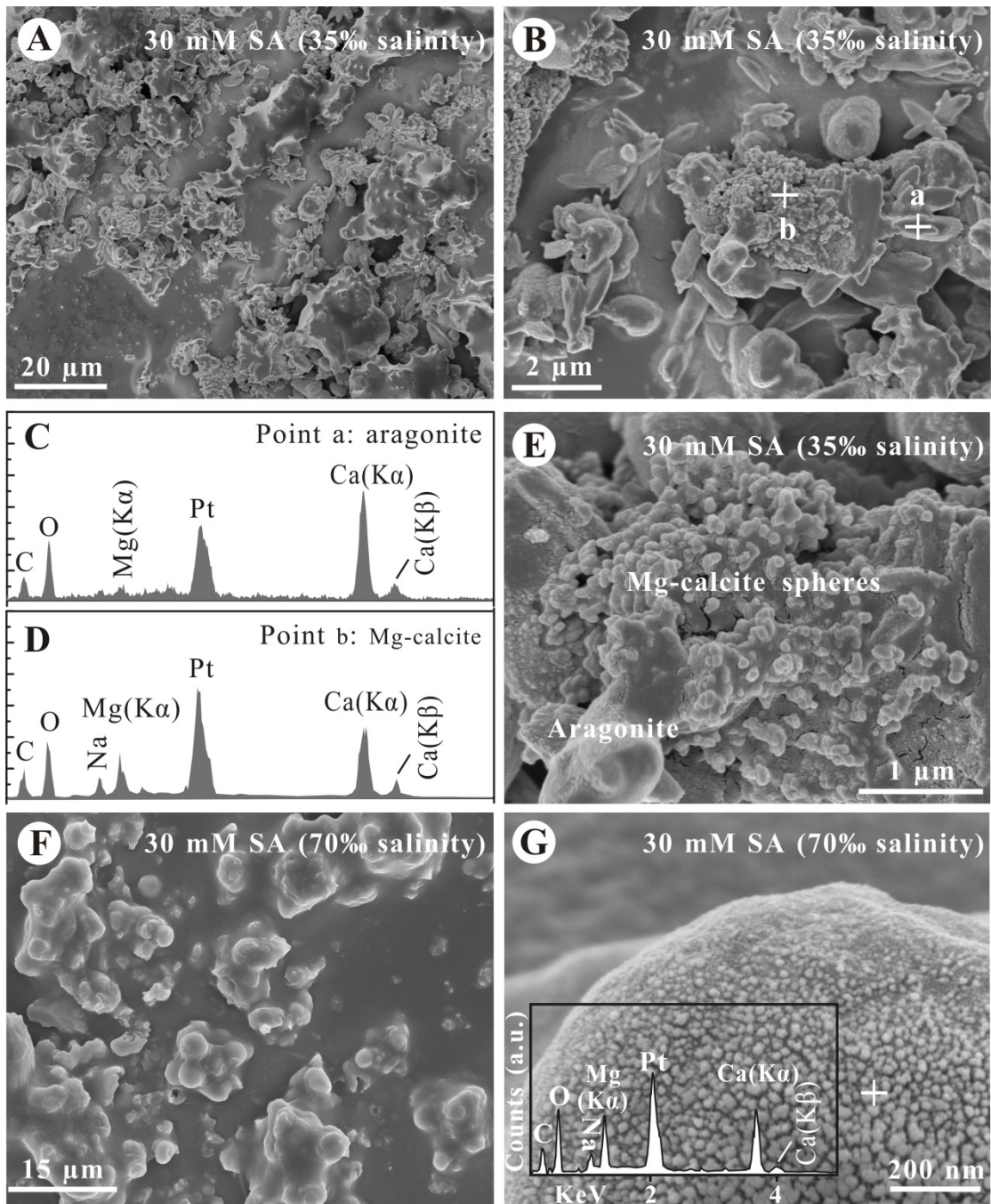
Figure 9
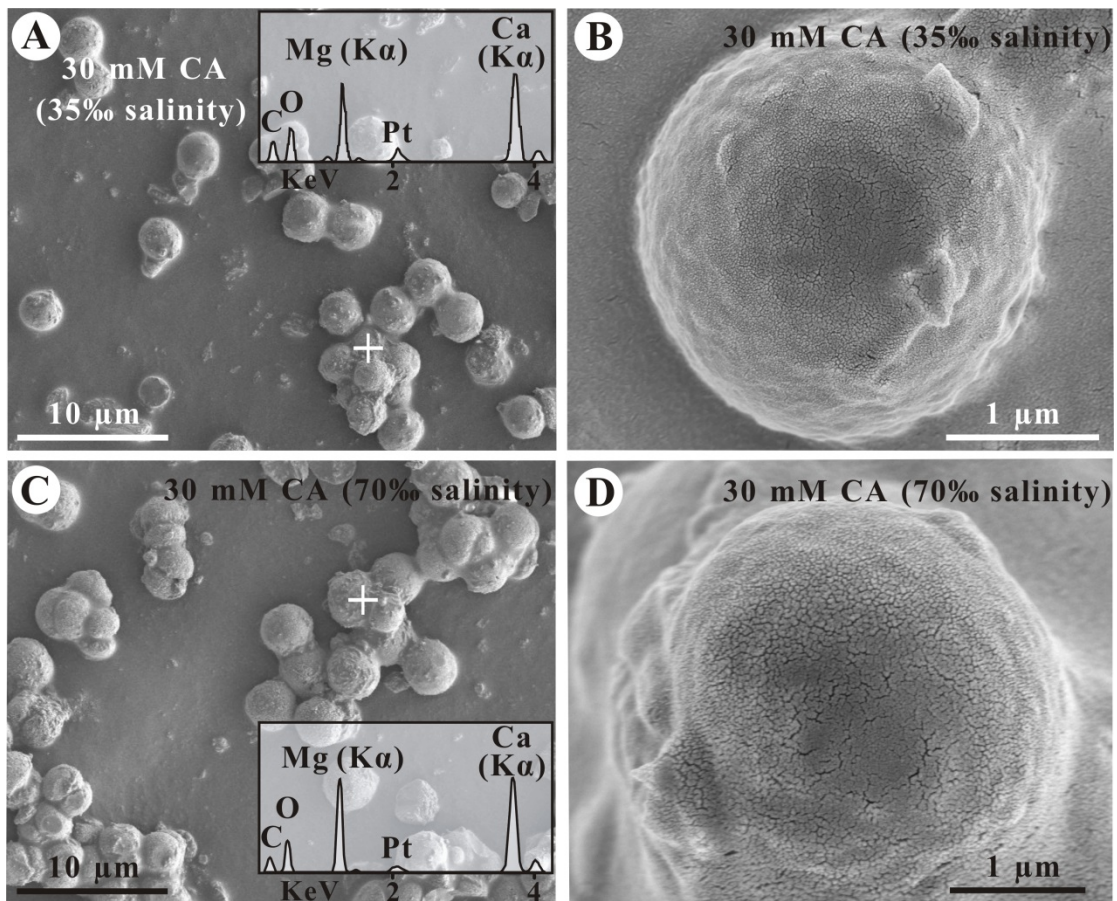
Figure 10

Figure 11

Figure 12